

GT2011-45) ) +

## LP TURBINE SECONDARY VORTICES: REYNOLDS LAPSE

**Matthias Kuerner, Georg A. Reichstein\*, Daniel Schrack,  
Martin G. Rose, Stephan Staudacher**  
Institute of Aircraft Propulsion Systems  
Stuttgart University  
Pfaffenwaldring 6  
D-70569 Stuttgart, Germany  
Email: reichstein@ila.uni-stuttgart.de

**Jochen Gier, Karl Engel**  
MTU Aero Engines GmbH  
Dachauer Strasse 665  
D-80995 Munich, Germany

### ABSTRACT

*A two-stage turbine is tested in a cooperation between the Institute of Aircraft Propulsion Systems (ILA) and MTU Aero Engines GmbH (MTU). The experimental results taken in the Altitude Test Facility (ATF) are used to assess the impact of cavity flow and leakage on vortex structures. The analysis focuses on a range of small Reynolds numbers, from as low as 35,000 up to 88,000. The five hole probe area traverse data is compared to steady multistage CFD predictions behind the second vane. The numerical model compares computations without and with cavities modeled. The simulation with cavities is superior to the approach without cavities. The vortex induced blockage is found to be inversely proportional to Reynolds number. The circulation of the vortices is dependent on the Reynolds number showing a reversing trend to smallest Reynolds numbers. The steady numerical model as of yet is unsuitable to predict these trends. A first unsteady simulation suggests major improvements.*

### NOMENCLATURE

$c$	absolute velocity [m/s]
$h$	specific enthalpy [J/kg]
$l/h$	relative annulus height [-]
$Ma$	Mach number [-]
$p$	pressure [Pa]

$R$	specific gas constant [J/(kg K)]
$Re_{v2}$	Reynolds number at exit of vane 2 [-]
$S$	non-dimensional pitch [-]
$T$	temperature [K]
$T_t$	stagnation temperature [K]
$U$	circumferential velocity [m/s]
$\vec{v}$	velocity vector [m/s]
$\gamma$	isentropic exponent [-]
$\eta_{is}$	isentropic efficiency [-]
$\eta_{row}$	blade row efficiency [-]
$\iota$	circumferential blockage factor, CBF [-]
$\vec{\omega}$	vorticity vector [1/s]
$\Gamma$	circulation [m <sup>2</sup> /s]

### INTRODUCTION

Over the past years the effect of Reynolds number on LP turbine flow has gained more and more attention. Motivated by high altitude applications where Reynolds numbers in LP turbines are as low as 50,000 in the final stage (see Hodson and Howell [1]) a better understanding of flows in such regimes is sought. From fluid dynamics in general, it is derived that laminar boundary layers dominate the flow field at low Reynolds numbers. Thus such a flow field consists of stronger secondary flows than one at higher Reynolds numbers. Horse-shoe vortices and passage vortices are but two of the effects that are expected to grow in

\*Address all correspondence to this author.

magnitude with decreasing Reynolds number. Furthermore the risk of laminar boundary layer separation without reattachment increases.

Experimental research faces the challenge of maintaining the Mach and Reynolds number analogy if a high grade of realism is to be achieved. A large quantity of the results published today are drawn from cascade experiments (i.e. Curtis *et al.* [2], Schulte and Hodson [3], Mahallati and Sjolander [4] or Volino [5]). Most cascades are limited to maintaining one of the two analogies. So called “closed loop turbine rigs” allow the experimental analysis of entire LP turbines under high altitude flight conditions. Few results of such experiments have been published in the past. Some are: Gier and Ardey [6], Haselbach *et al.* [7], Howell *et al.* [8], D’Ovidio *et al.* [9], Gier *et al.* [10] and most recent, Kürner *et al.* [11].

The results published by Kürner *et al.* [11] are based on the same experiment as those presented in this paper. Continuing the analysis the focus is again on the flow field after the second vane of the two stage turbine rig. In addition to previous results the analysis is now backed by computational results that include the cavity and leakage flows. The analysis starts with a comparison of row efficiency as a way of accessing flow structures and evaluating CFD results. At very low Reynolds numbers decreasing from 88,000 to 35,000 the analysis extends to a circumferential blockage factor and circulation to describe vortex structures at very low Reynolds numbers. The Reynolds number for this analysis is based on the exit velocity and the true chord length of the second vane. The steady multi-stage CFD calculations are performed without and with cavities and leakage to assess the importance of including these geometrical features in the analysis.

## DESCRIPTION OF THE TURBINE TEST RIG

The Advanced-Turbine-Research-Demonstrator-(ATRD)-Rig is a two-stage low pressure axial turbine at the Institute of Aircraft Propulsion Systems (ILA) at Stuttgart University. The ATRD-Rig operates in the Altitude Test Facility (ATF) at Reynolds numbers as low as  $Re_{V2} = 35,000$ . Thus it is possible to preserve both the Mach and Reynolds analogy for the turbine flow. This setup reproduces an LP turbine operated at high altitudes. Schinko *et al.* [12] give a very detailed description of the ATRD-Rig.

The setup under investigation in this paper is one of a series of different test builds. The series is intended to address various aspects of LP turbine flows at low and very low Reynolds numbers. Figure 1 shows a meridional view of the rig. The figure shows the annulus and cavities as included in the computational setup. The shaded sections mark the cavity geometry. Inlet and exit planes as well as the control volume boundaries ,1‘ and ,2‘ for the analysis of vane 2 are marked with dashed lines. For the computations without cavities the annulus is assumed to be

ideal without discontinuities in curvature. The computational setup without cavities does not include the shaded areas shown in Figure 1. In case of the ideal annulus the fillets are different from the actual annulus. The fillet radii are identical. For the ideal annulus the fillets extend further upstream than for the actual annulus because they do not drop into cavities.

The turbine blades have conventional blade loading and

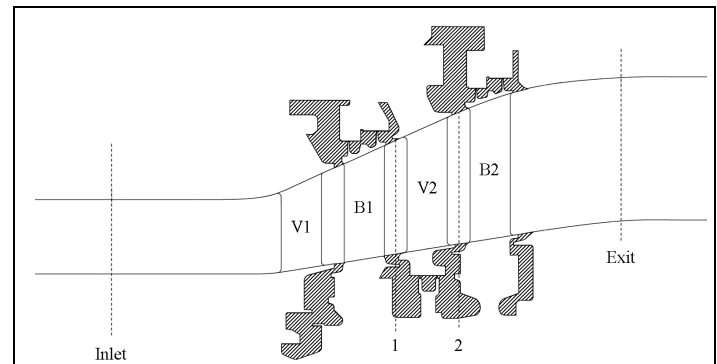


**FIGURE 1:** Meridional view of the ATRD-Rig as numerically modeled. Cavities (not included for ideal annulus analysis) are shaded.

typical aspect ratios (e.g. vane 2: 2.57). This compares well to state-of-the-art aft-loaded turbine blade designs, see Gier *et al.* [10]. On average, the Mach number at exit of each blade row is on the order of 0.6 and stage loading  $\Delta h_t/U^2$  is slightly above two. The radius ratio from the exit of vane 1 to the exit of vane 2 is 1.18. This results in an average flare angle on the order of  $17^\circ$ .

## EXPERIMENTAL METHODS

The reduction in efficiency due to Reynolds number is quantified using the isentropic efficiency,  $\eta_{is}$ . This efficiency is based on the stagnation flow values at inlet and exit of the turbine:

$$\eta_{is} = \frac{h_{t,inlet} - \hat{h}_{t,exit}}{h_{t,inlet} - h_{t,exit,is}} \quad (1)$$

Herein  $h_t$  ( $h_{t,is}$ ) represents the specific stagnation (isentropic) enthalpy. The gas properties are generally humidity corrected. Five hole probe area traversing was carried out for all operating conditions discussed herein.

At the exit the stagnation pressure,  $p_t$  and the stagnation temperature,  $T_t$ , are measured with three rakes each. Each rake is equipped with ten kiel heads, spaced to account for better resolution near the hub and the tip. The rakes are not placed

circumferentially equidistant to resolve circumferential flow distortions. Saravanamuttoo [13] provides detailed explanations on rake measurements in turbomachinery.

This paper focuses on steady five hole probe data in the measurement plane after the second vane. The five hole probe data was gathered using a traversing grid of 900 points per 1.1 pitches. For a detailed description of the area traversing methodology, see Kürner *et al.* [11]. The flow variables measured with the five hole probes are mass-averaged. The static pressure is area-averaged, see Cumpsty and Horlock [14].

## COMPUTATIONAL METHOD

The steady computational results presented here are obtained using TRACE, a 3D compressible Navier-Stokes solver. TRACE is based on a blockstructured finite volume scheme, see Franke *et al.* [15] and Eulitz *et al.* [16]. A second order central differencing scheme is applied to compute diffusive fluxes. The higher order MUSCL scheme in combination with Roe's flux differencing method [17] is used for convective fluxes, which are limited with a special version of the Van Albada Limiter.

Mixing planes couple the rotating and non-rotating parts of the computational domain. The mixing planes use flux averaging and are non-reflective interfaces, see Engel [18]. Full mass conservation across the mixing planes is enforced. The mixing planes are located at 50% of the blade spacing. Where necessary they stretch into the cavities. The mesh consists of about 5.7 million elements without cavities and 7.5 million with cavities. In the radial direction 117 nodes are applied. The leakage paths and seal geometry including gaps are based on the design geometry.

Turbulence is estimated by a two equation  $k-\omega$  model, see Röber *et al.* [19]. The low-Reynolds approach is applied to all surfaces, the blades, the endwalls and the cavities. Hence the  $y^+ \leq 1$  condition has to be satisfied on all surfaces. A quasi-unsteady model attempts to correct the downstream effect of blade rows on transition, which is averaged out by the mixing planes, see Kozulovic and Röber [20]. The cavity meshes are connected to the main passage via zonal interfaces, see Yang *et al.* [21].

For details on unsteady TRACE computations refer to Engel [18], Nürnberger *et al.* [22] or Yang *et al.* [23].

The static pressure at the exit is adjusted so that the calculated work of the turbine matches the experimental value, the latter being determined from temperature measurements at inlet and exit. Thus windage and bearing losses are of no concern.

## EXPERIMENTAL AND NUMERICAL RESULTS

### Turbine Characteristics

In Figure 2 the turbine characteristics for both stages in terms of isentropic efficiency,  $\eta_{is}$ , against Reynolds number of vane 2,  $Re_{V2}$ , are shown. The characteristic for the experimen-

tal results is compared to those based on the computations carried out with and without cavities. In the experiment the isentropic efficiency varies on the order of 3 percentage points with Reynolds number. This trend is slightly over predicted by the numerical results. Yet the difference between the experimental and the numerical result with cavities stays below 0.5%. The largest gap is observed at the highest Reynolds number. The offset between numerical simulations with and without cavities is of the order of 1.5 percentage points, the computational results without cavities overestimating the isentropic efficiency. As Kürner *et al.* [11] already stated, the decrease in isentropic efficiency with decreasing Reynolds number indicates an increase in losses. The trend is not linear, suggesting that with a further increase of Reynolds number its impact on isentropic efficiency will recede. Kürner

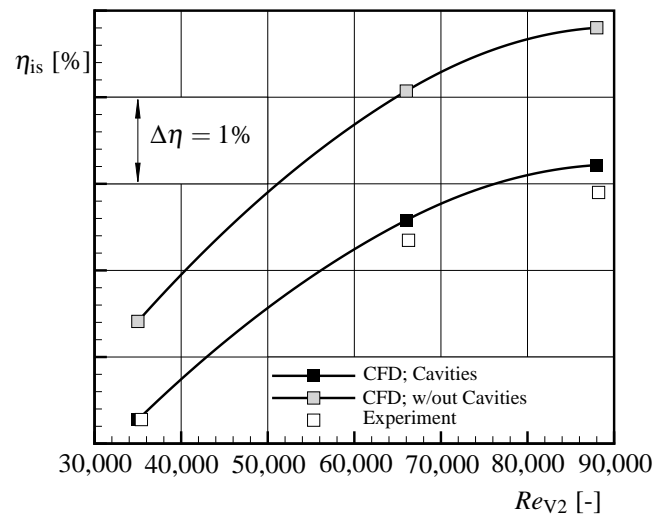


FIGURE 2: Isentropic efficiency,  $\eta_{is}$ , versus Reynolds number of vane 2,  $Re_{V2}$ .

*et al.* [11] discussed the variation of blade row efficiency with Reynolds number. Their analysis is the starting point for the results presented in this paper. Kürner *et al.* define the blade row efficiency as

$$\eta_{row} = \left( \frac{c_2}{c_{2,id}} \right)^2 \quad (2)$$

With  $c_{2,id}$  being the ideal isentropic exit velocity:

$$c_{2,id} = \sqrt{Ma_{id}^2 \cdot \gamma \cdot R \cdot T_{t,ref} \left( \frac{1}{1 + \frac{\gamma-1}{2} Ma_{id}^2} \right)} \quad (3)$$

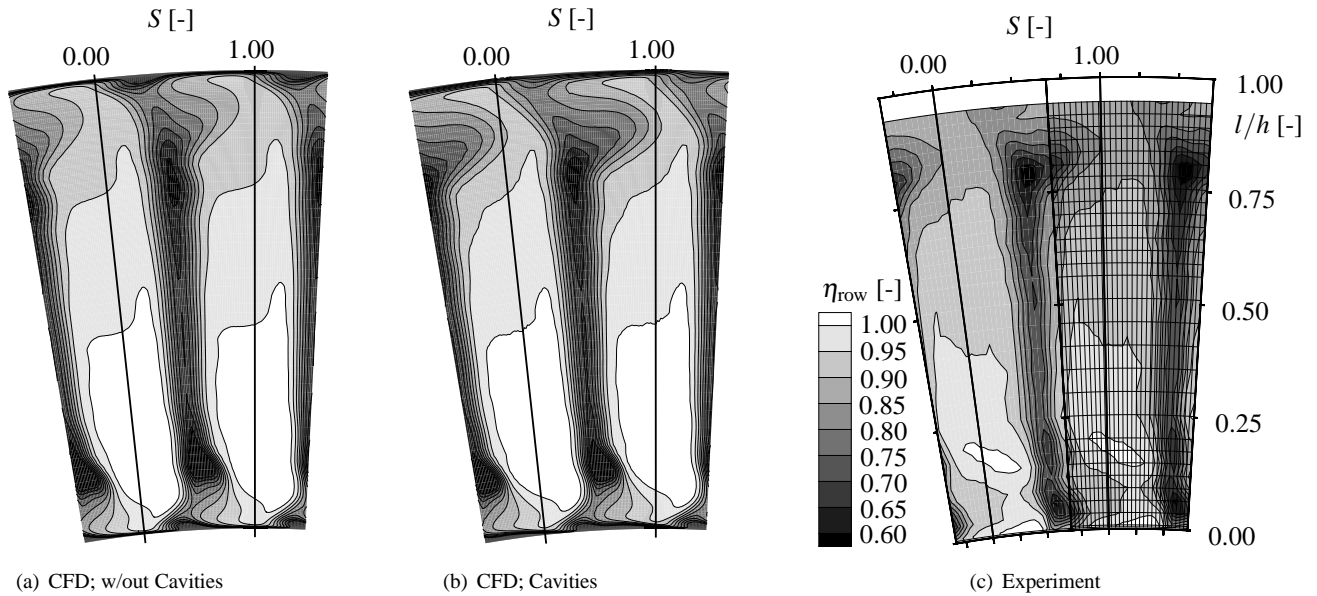


**FIGURE 3:** Blade row efficiency,  $\eta_{row}$ , at the lowest Reynolds number,  $Re_{V2} = 35,000$ . Experimental data shown with traverse grid and frame indicating annulus position. Position of trailing edge is marked for all cases.

$$Ma_{id}^2 = \frac{2}{\gamma - 1} \left[ \left( \frac{p_{t,ref}}{p_2} \right)^{\frac{\gamma-1}{\gamma}} - 1 \right] \quad (4)$$

The reference values  $T_{t,ref}$  and  $p_{t,ref}$  are obtained using kiel heads on the leading edge of vane 2 at midspan ( $l/h \approx 0.50$ ). The advantage of this definition of blade row efficiency over loss coefficients such as given by Denton [24] is that it takes pressure and temperature changes into account.

The distributions of row efficiency have been discussed at length in the previous paper by Kürner *et al.* [11]. Here only a comparison for the lowest Reynolds number is shown to illustrate the improvement gained by including cavities into the computational model. Figure 3 presents results for the measurement plane after vane 2. With the introduction of cavities to the computational setup the loss cores in the upper 25 % of the passage increase compared to the computation without cavities. The flow exiting the rotor cavity upstream of vane 2 distorts the flow in the casing region. This effect can be observed downstream of vane 2 and is supported by the experimental results as shown in Figure 3(c). In the lower 25 % of the passage the numerical results bear less resemblance to the experimental results than in the upper regions. The experiment resolves two loss cores in this region whereas both numerical approaches show only one, though larger, loss core. The loss cores in the experimental result are located at about 5 and 20 % radial height. This discrepancy hints at shortcomings of the current geometrical representation of the cavities, especially the seal gaps. Potential further improvement

of the numerical setup will be discussed in the following sections.

### Vortex Structures

The impact of cavity flow on vortex structures in the endwall regions of the annulus will be assessed using a circumferential blockage factor and circulation.

Integral parameters offer an attractive characteristic because noise (experimental error) and coarse resolution effects are mitigated. The classic integral boundary layer parameter “displacement thickness”, see Schlichting [25], can be misleading in the discussion of blockage between the blade rows. Based on the previous analysis by Kürner *et al.* [11] and the discussion below a “circumferential blockage factor” (CBF),  $\iota$ , is proposed. The CBF is mathematically the same definition as the integral boundary layer parameter,  $\delta_1$ .

**Vortex Induced Blockage.** Equation 5 gives the definition of the circumferential blockage factor,  $\iota$ , that is used in the subsequent analysis:

$$\iota = \int_0^S \left( 1 - \frac{c_2}{c_{2,id}} \right) ds \quad (5)$$

The ideal isentropic exit velocity is defined in equation 3. The integration was performed over one pitch at each height of the computational and traverse grid respectively. Figure 4(a) shows

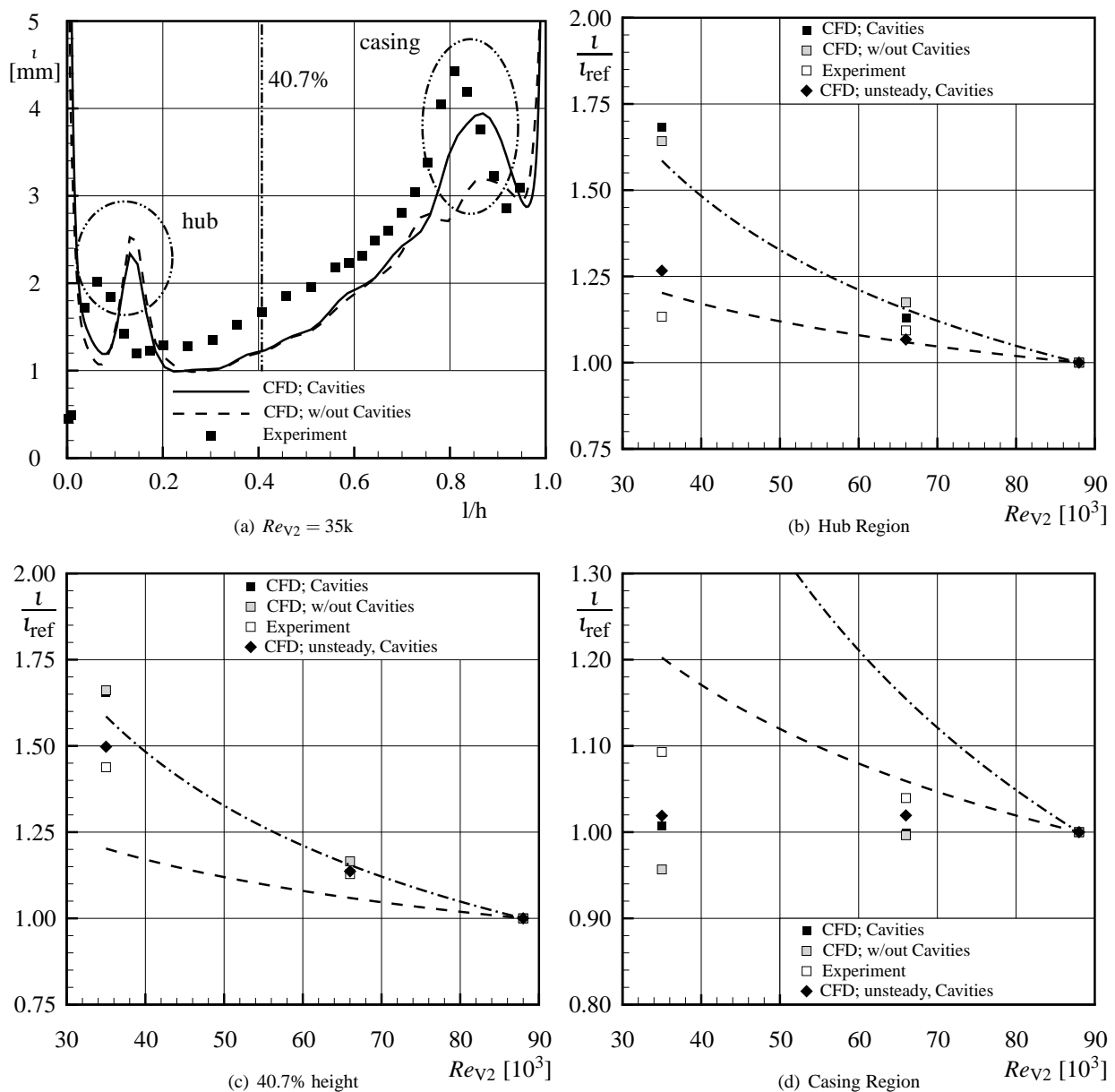


**FIGURE 4:** 4(a): Circumferential blockage factor over relative height;  $Re_{v2} = 35k$ ; (---) marks regions of analysis. 4(b)-4(d) Normalized circumferential blockage factor,  $\iota$ , over Reynolds number of vane 2,  $Re_{v2}$ . Values are relative to the respective CBF at the highest Reynolds number. (- -) indicates turbulent estimate,  $Re^{-0.5}$ ; (- · -) indicates laminar estimate,  $Re^{-0.2}$ .

a typical result. For the lowest Reynolds number of 35,000 the CBF is shown over the annulus height for both numerical cases and the experimental data. The bulk gradient stems from the use of a single reference value of  $T_{t,ref}$  and  $p_{t,ref}$  at midspan at the leading edge. These quantities experience a radial gradient which is not reflected in the evaluation of the circumferential blockage factor.

The steady CFD underpredicts the CBF on average by as much as 50 % between 25 and 75 % of the channel height. For the vortex structures in the endwall regions, indicated by peaks in the distribution of the CBF, the steady CFD results that include cavities bear closer resemblance to the measured data. This effect is also observed by D'Ovidio *et al.* [9]. In their analysis a two stage turbine was examined and modeled with and without

cavities. They too found that the representation of cavity flows in the computational model improved the results significantly yet the absolute location of the vortex structures was not accurately predicted. In summary, figure 4(a) shows that for the steady CFD results radial migration is too strong at the hub and too weak at the casing.

Conversely the trend lines in figures 4(b) and 4(d) appear to tell a different tale. Figure 4(b) hub steady CFD shows more blockage build up even though radial migration is stronger. Figure 4(d) casing, on the other hand, shows reduced blockage build up in the steady CFD along with underestimating radial migration.

The shift of the vortex structure closer to the hub in the experimental results compared to the steady CFD indicates that the mass flow into the cavity upstream of vane 2 is underestimated leading to a radially inward shift of the vortex. Similarly in the casing region the outflow of the rotor cavity upstream of the second vane is lower than for the experiment. Thus the impact on the main flow and the developing vortex structure is limited in the computational results. The vortex is predicted closer to the endwall. Yet the introduction of cavities has improved the computational results with regard to the experiment and lead to a shift towards the experimental data. Generally CFD tends to under predict radial migration in part due to the Boussinesq assumption of isotropic turbulent viscosity.

The Reynolds number trend for the circumferential blockage factor,  $\iota$ , is shown in Figures 4(b) to 4(d). The circumferential blockage factor values are shown relative to their respective value at the highest Reynolds number. The additional trend lines give an estimate based on flat plate isobaric correlations for boundary layer thickness development, see Dixon [26]. These lines are intended to act as a rough guide to the flowstate. Though the theoretical trends are derived from flat plate correlations they provide a realistic idea of the blockage when compared to the experimental results. The dashed line indicates a turbulent estimate:

$$\delta_{1,turb} \sim Re^{-\frac{1}{5}} \quad (6)$$

and the dash-dotted line gives the corresponding laminar estimate:

$$\delta_{1,lam} \sim Re^{-\frac{1}{2}} \quad (7)$$

For the wake region (around 40 % of the passage height, Figure 4(c)) the observed trend is closer to the laminar estimate than to the turbulent, indicating a transitional aerofoil. The computational results mirror that trend yet deviate increasingly with the reduction of Reynolds number. The circumferential blockage factor in the wake region appears unaffected by the introduction

of cavities.

In the hub region the respective peaks in the circumferential blockage factor distribution are compared. Here the experimental data suggests turbulent flow structures at the hub. The steady CFD results are unable to reproduce this behavior. Their trend follows the laminar estimate. Again the cavity flow has little impact on the vortex structures and the circumferential blockage factor.

Near the casing (Figure 4(d)) the computations with cavities resemble the experimental results more closely. The indifference with regard to Reynolds number predicted by steady CFD cannot be confirmed by the experimental data, though. Here the flow is calculated fully turbulent, yet the computations with and without cavities do not pick up a Reynolds number trend to increasing blockage. The computations without cavities even show a reversed trend towards less blockage with lower Reynolds numbers. The computational results are likely to be limited by the steady approach. Neglecting wakes by circumferential averaging and removing the unsteady pulsation that often occurs in combination with cavity flows (i.e. as mentioned by Boudet *et al.* [27]) lead to a simplified view. The boundary layer structures and turbulence levels in the endwall region are affected by the mixing plane which stretches into the cavities.

Due to space and time constraints this paper is limited to the reporting of only steady CFD results. However, an unsteady numerical analysis is also being carried out. On balance it was felt that some preliminary results of the time average of the unsteady solution would add to the value of this paper. These results are represented by the diamond symbols in Figure 4(b) - 4(d). At the hub and mid span height the offset between the numerical results and the experiment can be reduced on the order of 80 %. At the casing a similar but weaker trend can be observed suggesting that the build-up of blockage at the casing is indeed a quasi-steady effect. This early view of these developing unsteady CFD results encourages the view that time resolution will offer a significant improvement in agreement between numerical prediction and experiment.

**Circulation of Vortices.** A second approach to evaluate the behavior of vortex structures as a function of Reynolds number is the analysis of circulation:

$$\Gamma = \oint \vec{v} ds \quad (8)$$

Circulation,  $\Gamma$ , is defined as the line integral of the velocity vector,  $\vec{v}$ , along a closed curve. In equation (8)  $s$  denotes the variable grid spacing along the integration boundary. Applying this method, the axial circulation is calculated. Two integration boundaries are chosen for this analysis, enclosing the hub and casing loss cores respectively, see Figure 5. The integration

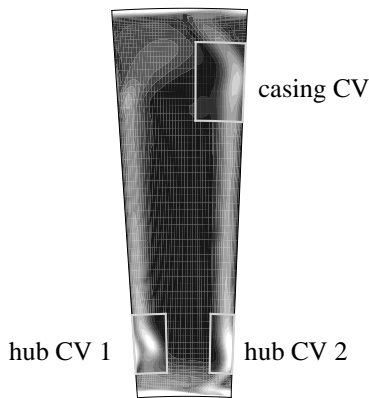


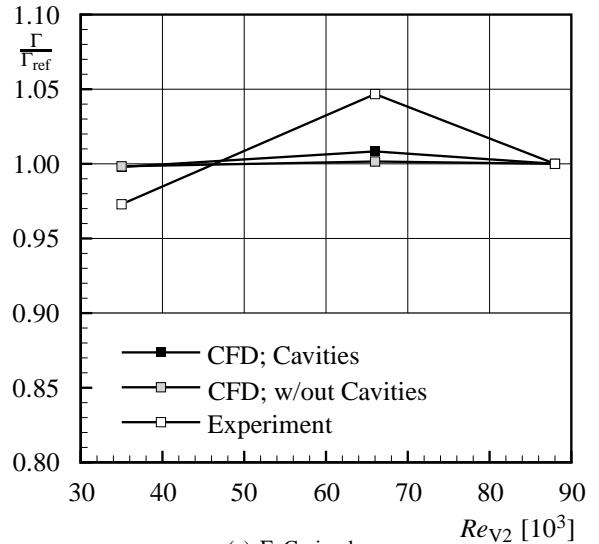
**FIGURE 5:** Boundaries of the control volumes (shown in grey) used to evaluate axial circulation.

boundaries follow the available grids and were varied to ensure that the non-dimensional result was independent of the control volume. The variation was on the order of 0.2 percentage points and concluded to be negligible. For the casing loss core the CFD predicts about 15 % more circulation than found in the experiment. For the hub loss core the CFD overestimates the circulation on the order of 70 % compared to the experimental data.

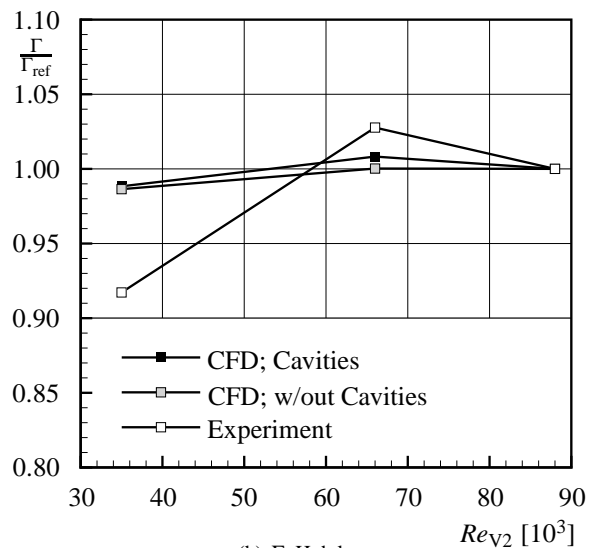
The hub and casing loss cores are regions where high loss fluid accumulates. There are many sources of this high loss fluid, most of them have streamwise vorticity and will contribute towards the measured circulation. In the test turbine at vane exit we can expect high loss fluid from the following sources: vane 2 horseshoe vortex, suction side and pressure side limbs, vane 2 passage vortex, vane 2 trailing shed vortex, unsteady remains of vane 1 vortices and rotor 1 vortices. Further contributions to loss cores are hub and casing boundary layers as well as blade steady wakes which do not roll up into vortices. At the casing we will see effects due to rotor 1 tip leakage, the hub leakage will draw fluid out at hub in front of vane 2. This will reduce the accumulation of fluid in the hub loss core. All the above source (and reductions) of high loss fluid will carry different levels of streamwise vorticity – some are positive in sign and others negative. The steady CFD calculations will not see the vane 1 or rotor 1 influences. The relative intensities of the circulation in each loss source will change the circulation as will the mixing between vortices of opposite sign.

The results are presented in Figure 6. In either case the CFD results show at best a negligible trend with Reynolds number. The experimental results on the other hand vary on the order of ten percentage points.

With a decrease in Reynolds number from 88,000 to 66,000 the increase in circulation is on the order of 4 % and resembles the 5 % increase in the turbulent trend line discussed in the previous section. Further decreasing the Reynolds number to 35,000



(a)  $\Gamma$ ; Casing loss core



(b)  $\Gamma$ ; Hub loss core

**FIGURE 6:** Circulation,  $\Gamma$ , over Reynolds number of vane 2,  $Re_{v2}$ .

does not increase the circulation. Instead, the circulation decreases on the order of 8 %. In summary with lower Reynolds numbers the vortex structures in the passage do increase. Being of opposite sign they lead to more mixing and eventually the destruction of circulation at very low Reynolds numbers.

The comparison of the circulation of the hub loss cores to that of the casing loss core shows that the effects described above

are more prominent at the hub after the second vane. Again the numerical simulation cannot pick up a Reynolds number trend. The introduction of cavities leads to a change in circulation on the order of 1 %. Though the direction of this change agrees with the experiment this trend is far too small to be of significance.

The unsteady analysis (not included in Figure 6) show no improvement with regard to the numerical simulation picking up the experimental trend. The shear stresses in the direction of the flow (and therefore blockage) are well predicted. Vorticity and circulation are dependent on shear stresses perpendicular to the flow direction. As mentioned earlier, the Boussinesq assumption and little sensitivity to changes in Reynolds number in the turbulence model limit the ability of the numerical approach to correctly predict circulation.

## CONCLUSIONS

The analysis is based on experimental results from a two-stage LP-turbine test rig at very low Reynolds numbers. These results are backed by steady numerical simulations. Two numerical setups are compared. The first takes only an ideal annulus into consideration. Including cavities into the computational model increases the quality of the results. An immediate effect is that TRACE predicts the overall isentropic efficiency derived from cavity-computations very well, lying within 0.2 percentage points of the experimental results. Computations without cavities show an offset of about 1.5 percentage points.

By comparing blade row efficiency contour levels after vane 2 the improvement of the numerical simulation with the introduction of cavities is underlined. The regions of reduced blade row efficiency bear closer resemblance to the experimental shapes. Yet the hub region shows simplified structures. A new parameter is introduced to clarify the analysis. The circumferential blockage factor, denoted  $\iota$ , is mathematically the same definition as the classic integral boundary layer parameter displacement thickness,  $\delta_1$ . It avoids misunderstandings with the classic boundary layer theory. The difference in the casing and hub passage vortex between the experimental results and the computational prediction are more clearly visible in the comparison of the circumferential blockage factor for the cases under examination. The numerical simulation under predicts the displacement thickness over the entire height of the passage. Furthermore the peaks of displacement thickness which are associated with vortices are radially shifted. This shift can be linked to cavity flows. The numerically predicted cavity flows are concluded to be lower than the estimates based on experimental radial displacement distributions. This causes a radial shift towards mid height for the vortex structures at the hub after the second vane. The vortex structures at the casing after vane 2 are shifted radially outward due to a lower mass flow in the outer cavities.

The steady numerical setup predicts a transitional aerofoil at

midheight which is supported by the experiment. Unfortunately turbulent trends at the hub and the casing are not picked up by the numerical model. In the hub region the numerical prediction is “too laminar” whereas at the casing it is “too turbulent”. The difference relative to trend lines may not be solely attributed to the offset in cavity mass flow. More likely the mixing plane approach in the steady computation averages out possible cavity jet flows.

The numerically predicted circulation is invariant with Reynolds number. The experiment shows a clear trend variation of circulation with changes in Reynolds number. Decreases from Reynolds number 88,000 to 66,000 causes an increase in circulation as vortices grow and become more potent. With a further decrease in Reynolds number to 35,000 circulation is destroyed. At very low Reynolds numbers more mixing occurs and counter rotating vortex structures counteract each other causing a reduction in circulation.

The numerical setup was improved with the inclusion of cavities. Based on the comparison of the row efficiency contours the numerical predictions bear good resemblance on a qualitative level to the experimental results. A more in depth analysis of the circumferential blockage factor and circulation to assess vortex structures reveal shortcomings of the current approach. The circumferential blockage factor is under predicted and unaffected by Reynolds number. The introduction of cavities currently does little to improve the numerical results in terms of circumferential blockage factor prediction. The computational simulation does not pick up the strong trend of circulation with Reynolds number. Here, the introduction of cavities hints at a possible improvement. These results are not believed to show shortcomings of the solver but the setup. Available results from an unsteady simulation show a great improvement of the results. This improvement supports the assumption that the solver is capable of resolving the flow with an improved setup. Future work will expand the unsteady analysis.

## ACKNOWLEDGMENT

The presented paper was developed as part of the Advanced Turbine Research and Demonstrator Project. The project is part of the Turbine Competence Center at Stuttgart University. Founded in 2006 it has since been a fruitful cooperation between MTU and Institutes at Stuttgart University.

The authors would like to express their gratitude and thanks to MTU for their continuous and valuable support. The authors are grateful for the opportunity to publish results from the research cooperation.

The authors thank the German government for providing the funding through LuFo IV.

## REFERENCES

- [1] Hodson, H.P.; Howell, R.J.: "Bladerow Interactions, Transition, and High-Lift Aerofoils in Low-Pressure Turbines", *Annu. Rev. Fluid Mech.*, 2005, Vol. 37
- [2] Curtis, E.M.; Hodson, H.P.; Banieghbal, M.R.; *et al.* : "Development of Blade Profiles for Low-Pressure Turbine Applications", *Journal of Turbomachinery*, 1997, Vol. 119
- [3] Schulte, V.; Hodson, H.P.: "Unsteady Wake-Induced Boundary Layer Transition in High Lift LP Turbines", *Transactions of the ASME*, 1998, Vol. 120
- [4] Mahallati, A., Sjolander, S.A.: "Aerodynamics of a Low-Pressure Turbine Airfoil at Low-Reynolds Numbers Part 2: Blade- Wake Interaction", *Proceedings of ASME*, GT2007-27348
- [5] Volino, R.J.: "Separated Flow Measurements on a Highly Loaded Low-Pressure Turbine Airfoil", *Journal of Turbomachinery*, 2010, Vol. 132
- [6] Gier, J.; Ardey, S.: "On the Impact of Blade Count Reduction on Aerodynamic Performance and Loss Generation in a Three- Stage LP Turbine", *Proceedings of ASME*, 2001-GT-0197
- [7] Haselbach, F.; Schiffer, H.-P.; Horsman, M.; *et al.* : "The Application of Ultra High Lift Blading in the BR175 LP Turbine", *Journal of Turbomachinery*, 2002, Vol. 124
- [8] Howell, R.J.; Hodson, H.P.; Schulte, V.; *et al.* : "Boundary Layer Development in the BR710 and BR715 LP Turbines - The Implementation of High-Lift and Ultra-High-Lift Concepts", *Journal of Turbomachinery*, 2002, Vol. 124
- [9] D'Ovidio, A.; Littlewood, L.; Congiu, F.; *et al.* : "Comparison Between Hot Wire and 5-Hole Pressure Probe Traverse Data in a Variable Density Two-Stages Air Turbine", *Proceedings of ASME*, GT2008-50753
- [10] Gier, J.; Franke, M.; Hübner, N.; Schröder, T.: "Designing LP Turbines for Optimized Airfoil Lift", *Proceedings of ASME*, GT2008-51101
- [11] Kürner, M.; Schneider, C.; Rose, M.G.; *et al.* : "LP Turbine Reynolds Lapse Phenomena: Time Averaged Area Traverse and Multistage CFD", *Proceedings of ASME*, GT2010-23114
- [12] Schinko, N.; Kürner, M.; Staudacher, S; *et al.* : "Das ATRD-Projekt - Ein Beispiel für die Zusammenarbeit von Industrie und Universität zur Förderung der Grundlagenforschung", *DGLR Congress, DLRK2009 121156*, Aachen 2009
- [13] Saravanamuttoo, H.I.H.: "Recommended Practices for Measurement of Gas Path Pressures and Temperatures for Performance Assessment of Aircraft Turbine Engines and Components", *AGARD Advisory Report No. 245*, 1990
- [14] Cumpsty, N.A.; Horlock, J.H.: "Averaging Nonuniform Flow for a Purpose", *Transactions of the ASME*, 2006, Vol. 128
- [15] Franke, M.; Kügeler, E.; Nürnberger, D.: "Das DLR-Verfahren TRACE: Moderne Simulationstechniken für Turbomaschinenströmungen", *DGLR-2005-211*, 2005
- [16] Eulitz, F.; Engel, K.; Nürnberger, D.; *et al.* : "On recent Advances of a Parallel Time-Accurate Navier Stokes Solver for Unsteady Turbomachinery Flow", 4<sup>th</sup> *ECOMAS Proceedings in Computational Fluid Dynamics*, Ed. Papailiou *et al.*, Vol. 1, Part 1, J. Wiley & Sons, 1998
- [17] Roe, P.L.: "Approximate Riemann Solvers, Parameter Vectors, and Difference Schemes", *Journal of Computational Physics*, 1997, Vol. 135
- [18] Engel, K.: "Numerische Simulation der instationären Strömung in Turbomaschinenkomponenten", *Dissertation, Universität-GH Essen*, 1997
- [19] Röber, T.; Kozulovic, D.; Kügeler, E.; *et al.* : "Appropriate Turbulence Modelling for Turbomachinery Flows Using a Two- Equation Turbulence Model", *New Results in Numerical and Experimental Fluid Mechanics V*, Ed. Rath *et al.*, Springer, 2006
- [20] Kozulovic, D.; Röber, T.: "Quasi-unsteady transition modelling of periodic wakes", *Turbulence, Heat and Mass Transfer 5*, Begell House, New York, 2006.
- [21] Yang, H.; Nürnberger, D.; Nicke, E.; *et al.* : "Numerical Investigation of Casing Treatment Mechanisms with a Conservative Mixed-Cell Approach", *Proceedings of ASME*, 2003-GT-38483
- [22] Nürnberger, D.; Eulitz, F.; Schmitt, S.; *et al.* : "Recent progress in the Numerical Simulation of unsteady viscous multistage turbomachinery flow", *ISABE 2001-1081*
- [23] Yang, H., Nürnberger, D., Weber, A.: "A Conservative Zonal Approach with Applications to unsteady Turbomachinery Flows", *DGLR-2002-073*
- [24] Denton, J.D.: "Loss Mechanisms in Turbomachines", *Journal of Turbomachinery*, 1993, Vol. 115
- [25] Schlichting, H.; Gersten, K.: "Grenzschicht-Theorie", Springer, Berlin, 2006
- [26] Dixon, S.: "Fluid Mechanics, Thermodynamics of Turbomachinery", Third Edition, Butterworth-Heinemann, 1978.
- [27] Boudet, J.; Hills, N.J.; Chew, J.W.: "Numerical Simulation of the Flow Interaction Between Turbine Main Annulus and Disc Cavities", *Proceedings of ASME*, GT2006-90307